A MEMS Coriolis-Based Mass-Flow-to-Digital Converter with 100g/h/surdHz Noise i Floor and Zero Stability of pm 0.35mg/h

Oliveira, Arthur C. de; Pan, Sining; Makinwa, Kofi A. A.

DOI
10.1109/ISSCC42614.2022.9731704

Publication date
2022

Document Version
Final published version

Published in
2022 IEEE International Solid- State Circuits Conference (ISSCC)

3.6 A MEMS Coriolis-Based Mass-Flow-to-Digital Converter with 100μg/h/√Hz Noise Floor and Zero Stability of ±0.35mg/h

Arthur C. de Oliveira, Sining Pan, Kofi A. A. Makinwa

Delft University of Technology, Delft, The Netherlands

Flow sensors with high resolution (<200μg/h/√Hz) and low offset drift (<±0.4mg/h) are essential in many microfluidic applications, such as flow cytometry and biological/chemical assays. Although thermal flow sensors can meet these specifications [1,2], they measure flow velocity, so their calibration is fluid specific. Coriolis flow sensors [3-5] are a promising alternative because they measure mass flow and density regardless of fluid type, thus offering more flexibility. However, this has typically been at the expense of lower resolution, offset drift, and large footprint. This paper presents a mass-flow-to-digital converter (ΦDC) based on a MEMS Coriolis mass flow sensor and a dedicated readout IC (ROIC). Compared to the state-of-the-art [5], it is more compact and has a digital output. Furthermore, it achieves a 3× improvement in resolution (100μg/h/√Hz) and a more than 2× improvement in zero stability (±0.35mg/h).

Figure 3.6.1 shows the system block diagram of the proposed ΦDC. It consists of a MEMS Coriolis flow sensor and an ROIC that realizes a drive loop and a sense readout. The sensor consists of a micromachined flow channel suspended in a magnetic field B, which is driven into oscillation around its drive axis (twist mode) by passing a current (I_{DRIVE}) through a metal coil deposited on top of the channel. In the presence of mass flow (Φ) through the sensor's channel, a Coriolis force directly proportional to it, and orthogonal to the drive axis, excites its sense axis (swing mode). The resulting drive and sense motions are detected by the drive and sense capacitances (comb electrodes), $C_{D1,2}$ and C_S, respectively, attached to the channel.

The function of the drive loop is to drive the suspended flow channel at its resonance frequency f_D. It consists of a capacitance-to-voltage (C/V) converter followed by a PLL and an amplitude regulator that maintains constant oscillation amplitude by regulating the drive capacitance change (ΔC_D). Compared to [5], in which drive amplitude was sensed via the emf generated in a secondary coil, this approach reduces drive-loop complexity and can simplify the manufacture of the flow channel.

The sense readout digitizes changes (ΔC_S) in the sense capacitance (C_S). Ideally, due to its symmetrical placement around the drive axis, C_S should only detect Coriolis-force induced motion. However, manufacturing tolerances will give rise to some mechanical asymmetry, and so a portion of the drive motion will couple to the sense axis and cause flow-independent variations in C_S. This mechanical crosstalk can be a significant source of sensor drift. Since the crosstalk has a 90° phase shift relative to the Coriolis signal, it is commonly referred to as quadrature error [6,7]. In [5], mass flow is determined from the ratio of the in-phase (I) and quadrature (Q) components detected by comb electrodes. However, the use of the quadrature signal degrades the zero stability (ZS), or offset drift, of the sensor, while the need for two sense channels increases its noise floor. In this work, the flow-induced ΔC_S are detected by a single C/V converter, which reduces readout noise by at least 3dB and improves the ZS.

The output of the sense C/V converter is digitized by two continuous-time delta-sigma modulators (CT-ΔΣMs) with embedded I and Q demodulators. As a result, the quadrature error can be continuously monitored, together with the extra phase-delay (φ) due to the finite Q-factor of the sense mode and the limited bandwidth of the sense readout channel. The latter can then be canceled by combining the I and Q components with the appropriate weights ($\cos\varphi$ and $\sin\varphi$) [6]. This further improves the system's ZS and only requires a 1-point calibration.

The mass flow sensitivity of a MEMS Coriolis sensor is directly proportional to f_D, which means that its sensitivity drops as a function of fluid density. In [5], this effect is compensated in the digital domain by normalizing the sensor's output by f_D and performing a 1-pt gain calibration. However, this led to different noise floors and ZS for liquids and gases. Here, the compensation is implemented in the analog domain. By measuring changes in f_D, an off-chip background sensitivity tuning (BST) block linearly adjusts the nominal HV-bias (~20V) of the sense capacitors, thus matching the sensor's sensitivity for liquids and gases and achieving a similar noise floor and ZS for all fluids.

Figure 3.6.2 shows a simplified schematic of the drive loop, which consists of start-up, amplitude, and frequency-control paths. In contrast to [5], they are all fully integrated. The drive capacitances are read out by a low-noise (~12fA/√Hz) capacitive transimpedance amplifier (C-TIA) with a gain of 154 to 148dBΩ at f_D (1.8 to 3kHz). During the start-up phase (Φ_{ST}), the C-TIA is followed by a differentiator, which adds a 90° phase shift to ensure oscillation, and a driver provides the initial drive current I_{DRIVE} to the sensor. An embedded charge-pump (CP)-PLL then locks to f_D and provides all the clocks used in the drive loop, as well as the I/Q clocks to demodulate the sense C/V output. Once the PLL locks, the start-up path is disabled, and the frequency and amplitude-control paths take over. During normal operation, the C-TIA output is buffered and boosted by capacitively coupled amplifiers, which also block its DC offset. The amplitude-control loop is built around a switched-capacitor (SC) proportional-integral (PI) controller, which consists of a flip-around synchronous amplitude detector [7], followed by a correlated-double-sampling (CDS) integrator. Both circuits suppress 1/f noise of the amplitude controller and thus improve the sensor's long-term stability [5,8]. The proportional and integral gains are set by resistors R_P and R_I, which are connected to the driver's virtual ground. The resulting control currents are then up-modulated to f_D and summed by the driver to provide i_{DRIVE} at steady state, whose amplitude is defined by the reference voltage V_{REF}.

The sense C/V is a single-ended version of the drive C/V. As shown in Fig. 3.6.3, its output is digitized by the two I/Q ADCs. These are based on 1-bit 2nd-order CT-ΔΣMs with FIR-DACs [9], which are preceded by passive mixers. To achieve high linearity, the voltage swing across the mixer switches should be minimized by making their on-resistance (r_{on}) small compared to R_{IN}. In addition, the use of a 4-tap FIR-DAC significantly reduces the swing at the 1st integrator's virtual ground. Exploiting the notches of the FIR-DAC, the 1st integrator is chopped at $f_s/8$ to mitigate its offset and 1/f noise without incurring quantization noise folding. The resulting bitstreams (BS_I and BS_Q) are decimated off-chip and then recombined to realize a low-drift mass flow output.

Realized in a standard 0.18μm CMOS process, the ROIC (Fig. 3.6.7, left) occupies 4.84mm² and draws 7.2mA from a 1.8V supply. The MEMS Coriolis mass flow sensor (Fig. 3.6.7, right) was fabricated using a bulk-micromachining surface-channel technology to realize a flow channel with 60μm diameter and 1.2μm thick walls. With the help of a custom 3-D printed fluidic connector, the complete ΦDC was characterized for several liquids (H_2O, IPA, 50/50 H_2O+IPA) and gases (N_2, Ar, CO_2).

Figure 3.6.4 (top left) shows the decimated output of a typical sample for mass flows up to 5g/h. After a 1-pt trim at 2g/h for H_2O and N_2, the sensor's sensitivity is tuned in the background during normal operation, resulting in a sensitivity variation of less than 2.3% for all fluids (Fig. 3.6.4, top right). Fluid density can be determined from the inverse square of the PLL's output frequency (128×f_D), which, as expected, is a linear function of density (Fig. 3.6.4, bottom). The output noise spectrum of the combined bitstreams BS_I and BS_Q is shown in Fig. 3.6.5 (top), for both N_2 and H_2O under zero flow conditions. In both cases, this results in a mass flow noise floor of 100μg/h/√Hz. After correcting for the quadrature error, the ZS (±0.35mg/h) over a 1-hour interval is also the same for both cases, as shown in Fig. 3.6.5 (bottom).

The performance of the ΦDC is compared to that of other state-of-the-art flow sensors in Fig. 3.6.6. It achieves the highest dynamic range, by about 10dB. Compared to a state-of-the-art MEMS Coriolis mass flow sensor [5], it has a digital output, and its noise floor and ZS are 3× and 2.3× lower, respectively, and remain the same for all fluids. In terms of noise floor and ZS, the proposed sensor even outperforms MEMS thermal flow sensors [1,2]. These results show that MEMS Coriolis mass flow sensors can now replace MEMS Thermal flow sensors in many low-flow microfluidic applications with fluid agnostic performance.

Acknowledgment:
The authors would like to thank the Dutch technology foundation STW, Bronkhorst BV, and KROHNE Nederland BV for financial support. We would also like to thank L. Pakula, Z. Chang, and R. van Puffelen for their help with the design of the measurement setup, and J. Groenesteijn and R. Wiegerink for providing the sensor elements.

References:
[1] Sensirion AG, SLG-0025 Liquid Flow Meter Datasheet, Mar. 2019.
[2] M. Ahmed et al., "Fully Integrated Bidirectional CMOS-MEMS Flow Sensor with Low Power Pulse Operation," *IEEE Sensors J.*, vol. 19, no. 9, pp. 3415-3424, May 2019.
[3] Bronkhorst BV, mini CORI-FLOW™ Series ML120 Coriolis Mass Flow Meter Datasheet, Nov. 2019.
[4] R. Smith, et al., "A MEMS-Based Coriolis Mass Flow Sensor for Industrial Applications," *IEEE Trans. Industrial Electronics*, vol. 56, no. 4, pp. 1066-1071, Apr. 2009.
[5] A. C. de Oliveira, et al., "A MEMS Coriolis Mass Flow Sensor with 300μg/h/√Hz Resolution and ±0.8mg/h Zero Stability," *ISSCC*, pp. 84-85, Feb. 2021.
[6] C. Ezekwe et al., "A 3-Axis Open-Loop Gyroscope with Demodulation Phase Error Correction," *ISSCC*, pp. 478-479, Feb. 2015.
[7] B. Eminoglu and B. Boser, "Chopped Rate-to-Digital FM Gyroscope with 40ppm Scale Factor Accuracy and 1.2dph Bias," *ISSCC*, pp. 178-179, Feb. 2018.
[8] X. Wang et al., "A 1.2μg/√Hz-Resolution 0.4μg-Bias-Instability MEMS Silicon Oscillating Accelerometer with CMOS Readout Circuit," *ISSCC*, pp. 476-477, Feb. 2015.
[9] S. Pan and K. A. A. Makinwa, "A Wheatstone Bridge Temperature Sensor with a Resolution FoM of 20fJK²," *ISSCC*, pp. 186-188, Feb. 2019.

2022 IEEE International Solid-State Circuits Conference (ISSCC) | 978-1-6654-2800-2/22/$31.00 ©2022 IEEE | DOI: 10.1109/ISSCC42614.2022.9731704

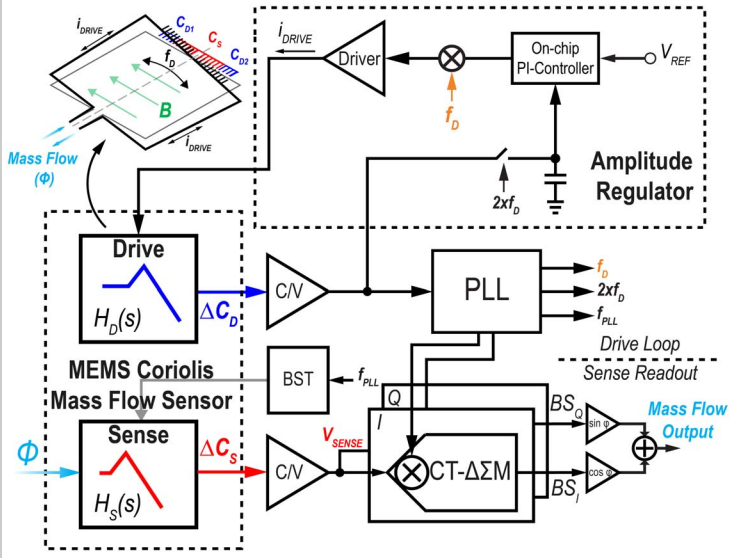

Figure 3.6.1: System block diagram of the mass-flow-to-digital converter.

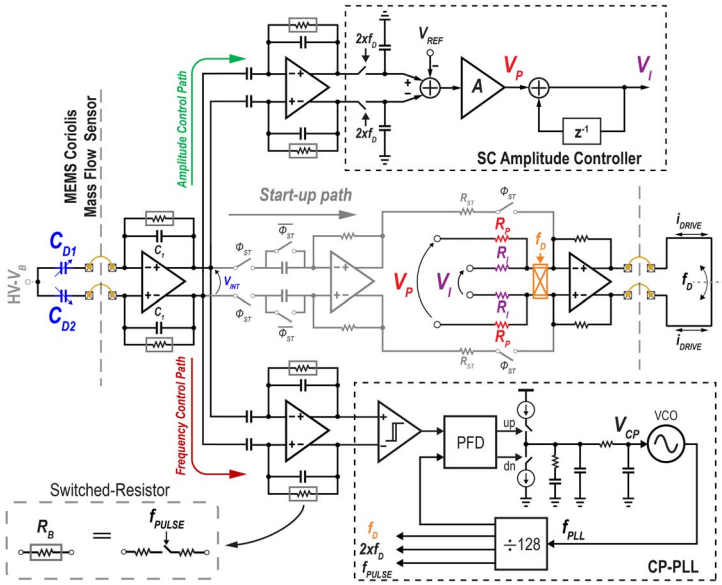

Figure 3.6.2: Simplified circuit diagram of the drive loop.

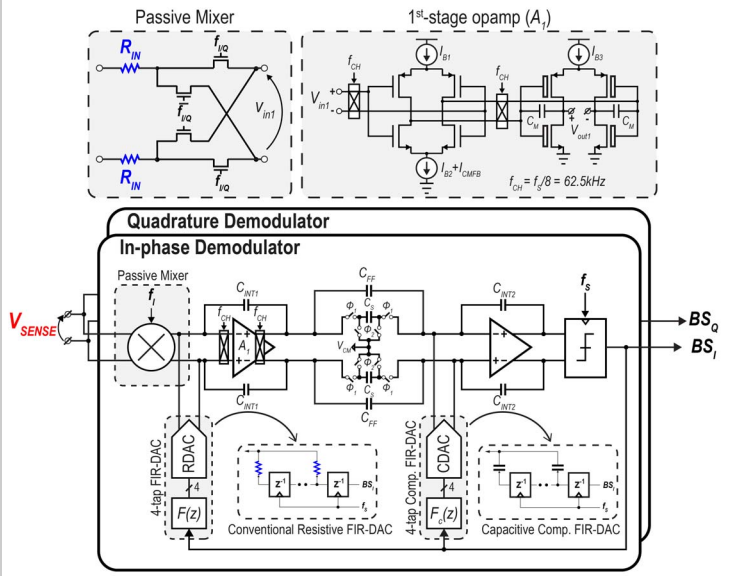

Figure 3.6.3: CT-ΔΣM sense readout with embedded passive IQ demodulator.

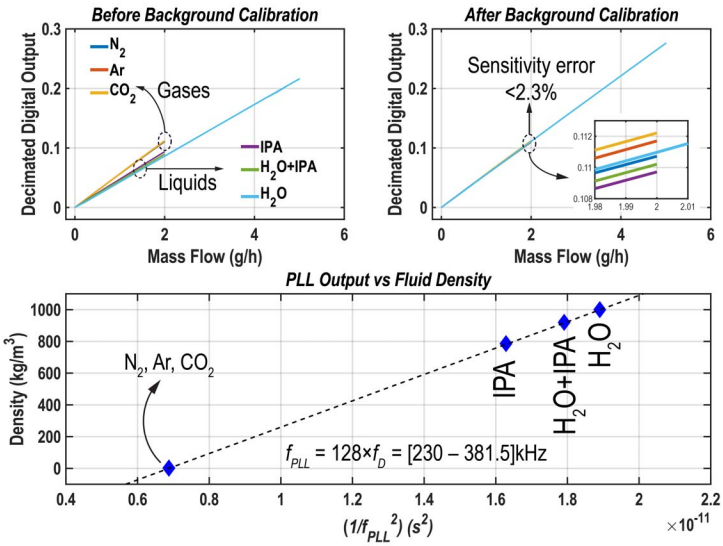

Figure 3.6.4: Measured sensor output (top left); sensor output after sensitivity tuning using H_2O and N_2 (top right); fluid density versus $(1/f_{PLL})^2$ (bottom).

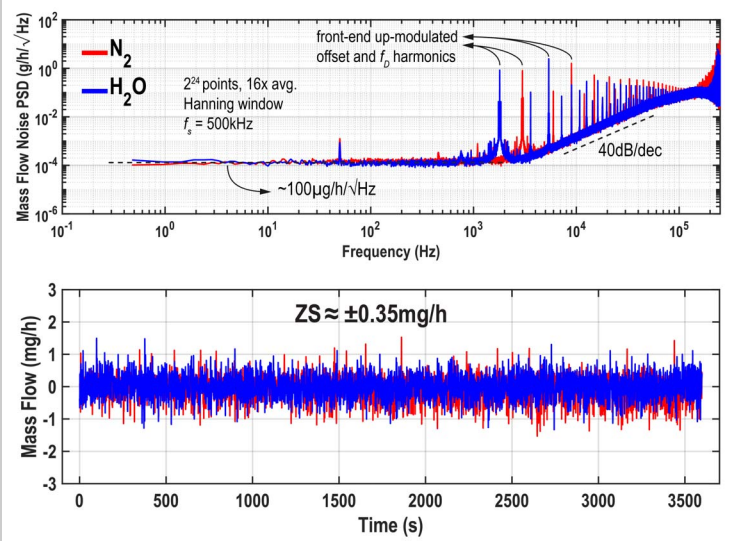

Figure 3.6.5: Measured output noise spectrum (top); sensor's zero stability with N_2 and H_2O (bottom).

	[1]	[2]	[3]	[4]	[5]	This Work
Sensor Type	MEMS Thermal	MEMS Thermal	SS Coriolis	MEMS Coriolis	MEMS Coriolis	**MEMS Coriolis**
Readout Technology	CMOS	0.18µm CMOS	COTS	COTS	0.18µm CMOS	**0.18µm CMOS**
ASIC Output	Analog	Analog	-	-	Analog	**Digital**
Fluids	H_2O	N_2	Liquids & Gases	Liquids (H_2O)	Liquids & Gases	**Liquids & Gases**
Full Scale (g/h)	0.09	0.36[c]	5	500	5	**5**
Noise Floor (µg/h/√Hz)	<600[a]	<200	<4000[a]	N/A	300	**100**
Bandwidth (Hz)	4	25	3	1.6	3	**4**
Dynamic Range[b] (dB)	43.5	65.1	61.9	N/A	84.4	**94**
Zero Stability (mg/h)	N/A	N/A	±10	±223	±0.8	**±0.35**
Power Consumption (mW)	21.5	8.9	2500	400	14.6	**13**

[a]Estimated from repeatability. [c]Limited to the linear range.
[b]1Hz bandwidth. N/A = Specification not available

Figure 3.6.6: Performance summary and comparison with previous works.

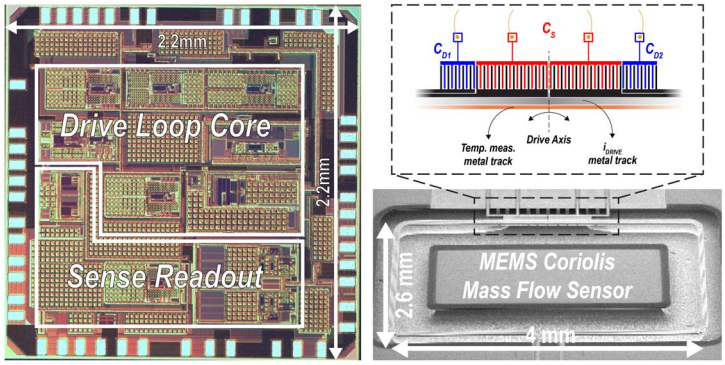

Figure 3.6.7: Micrograph of the 0.18μm CMOS die (left); MEMS SEM image and detailed readout capacitors (right).

978-1-6654-2800-2/22/$31.00 ©2022 IEEE